This is the Pre-Published Version.

D. Luan, R. Bu, Z. Sheng, C. Fan, X. Huang (2023) *Experimental study on the impact of asymmetric heavy rainfall on the smoke spread and stratification dynamics in tunnel fires*, **Tunnelling and Underground Space Technology**, 134, 104992. https://doi.org/10.1016/j.tust.2023.104992

Experimental study on the impact of asymmetric heavy rainfall on the smoke spread and stratification dynamics in tunnel fires

Dia Luan[1], Rongwei Bu[1], Ziqiong Sheng[1], Chuangang Fan[1,*], Xinyan Huang[2,*]

[1]*School of Civil Engineering, Central South University, Changsha, China*

[2]*Department of Building Environment and Energy Engineering, The Hong Kong Polytechnic University, Kowloon, Hong Kong, China*

*Corresponding to chuangang.fan@csu.edu.cn (CF), xy.huang@polyu.edu.hk (XH)

Abstract

This work examines the impact of heavy rainfall on the smoke spread and stratification dynamics in tunnel fires with a reduced-scale (1:15) experimental platform. Scaled tests vary the rainfall intensity (up to 60 mm/h, equivalent to 232 mm/h in nature), raindrop size (1.0-1.5 mm, equivalent to 4-6 mm in nature), and fire heat release rate (2.1-6.7 kW, equivalent to 2-6 MW in real scale). We found that the asymmetric rainfall on one exit can induce the longitudinal airflow inside the tunnel due to the dissipation of the raindrop momentum and the rain-induced air entrainment. The velocity of such a longitudinal airflow increases with increasing rainfall intensity, and smaller raindrops tend to induce faster longitudinal airflow. The spread and stratification of hot smoke are sensitive to the induced airflow. In the absence of rainfall, there was a symmetrical temperature distribution from the fire source due to the symmetrical air entrainment. Under rainfall, the temperature distribution of tunnel fires gradually becomes less symmetrical, and the smoke stratification interface becomes unclear. With the increase in rainfall intensity, the phenomenon of smoke back-layering appears, and the smoke layer height constantly decreases. Under a small rainfall intensity, raindrop size has a higher impact on the smoke stratification near the fire source. This study aims to attract more attention to tunnel safety under the dual disaster of fire and extreme weather and support the emergency response.

Keywords: *Weather effect; Tunnel safety; Temperature distribution; Smoke motion; Smoke layer; Rainfall intensity*

Nomenclature

A	pool area (cm^2)	W	tunnel width (m)
d	raindrop size (mm)	x	longitudinal distance to the rainfall portal (m)
d_0	median volume drops diameter (mm)	Δx	longitudinal distance to the fire source (m)
E	energy (kJ)	Z	height from the tunnel floor (m)
Fr	Froude number (-)	*Greek Symbols*	
h	smoke layer thickness (m)	γ	scale ratio, equals 15 in our test (-)
H	tunnel height (m)	ρ	water density (kg/m^3)
I	rainfall intensity (mm/h)	*Subscripts*	
L	tunnel length (m)	*max*	maximum value
N	value in the N-percentage method (-)	0	ambient condition
p_n	rainfall kinetic energy ($J/m^2.h$)	F	full tunnel
Q	heat release rate (kW)	M	model tunnel
r	integral ratio (-)	u	upper layer
ΔT	excess temperature (°C)	l	lower layer
ΔT_h	the maximal excess temperature (°C)	i	smoke layer interface
V	airflow velocity (m/s)		

1. Introduction

The tunnel, a crucial component of the transportation infrastructure, offers consumers great convenience by reducing traffic congestion and shortening travel time (Yang et al., 2019). However, due to the narrow and confined tunnel space, the risk of casualties and infrastructure damage is serious in the event of a tunnel fire (Zhang et al., 2021). Consequently, tunnel fire safety has received a lot of attention (Yan et al., 2017; Xu et al., 2019a). Previous research has looked into the influence of tunnel shape, ventilation conditions, and ambient pressure on tunnel fire dynamics. However, with climate change, extreme weather, like heavy rainfall, occurs with increasing intensity and frequency, which has become a new norm (IPCC, 2022). Consequently, the probability of tunnel fires occurring under heavy rainfall is increasing. Such dual disaster events could cause incalculable consequences. Therefore, it is necessary to understand the characteristics of tunnel fire under heavy rainfall and improve the capability of disaster prevention and emergency rescue in the tunnel.

Smoke is the main cause of casualties in fire accidents (Weng et al., 2015). Four regions, i.e. the rising plume region, the radial spread region, the transition region, and the one-dimensional horizontal spread region, can be used to categorize the smoke flow produced by fires in a long and narrow space (Kunsch, 1999). The smoke flow characteristics (e.g., temperature distribution, smoke stratification, smoke layer height) of tunnel fires have been extensively studied, particularly for the one-dimensional horizontal spread region.

Motevalli and Marks (1991) found that the thermal boundary and momentum boundary of the unconfined ceiling jet were not identical. They established a model to determine the smoke layer thickness as shown in Eq. (1),

$$h/H = 0.112\left[1-\exp\left(-2.24\Delta x/H\right)\right],\ for 0.26 \le \Delta x/H \le 2.0 \quad (1)$$

Newman (1984) found that forced longitudinal ventilation allowed sufficient mixing of upper smoke and lower air in a duct, and then, quantified the smoke stratification by Froude number (Fr). Lemaire and Kenyon (2006) performed several fire tests in the Benelux tunnel. They discovered that under longitudinal ventilation conditions, the thermal stratification of the downstream smoke was eliminated, resulting in a noticeable reduction in visibility. Hu et al. (2008) investigated the critical velocity of fires occurring near the sidewall using theoretical analysis and CFD simulations, revealing that a higher critical velocity is necessary to restrain the diffusion of upstream smoke when a fire occurs near the sidewall. The numerical simulations by Wu et al. (2018) showed that the back-layering length increased with decreasing ambient pressure. Ji et al. (2017; 2018) further showed that with the decreasing ambient pressure, the field temperature increased, and the smoke mass flow rate decreased. More recently, Luan et al. (2021) analyzed the smoke spread characteristics of tunnel fires influenced by asymmetric canyon crosswind, and found that the airflow barrier effect formed by canyon crosswind would prevent the smoke from escaping. Guo et al. (2021) proposed a concept of "stratification velocity" as the highest velocity to sustain downstream smoke stratification and found that Fr = 0.49 can be applied to judge whether downstream smoke stratification is maintained. Gao et al. (2022) numerically analyzed the ceiling temperature profile and thermal smoke behavior in inclined tunnel fires. It was found that the temperature profile was asymmetrical, and the maximum ceiling temperature decreased with the increase of tunnel slope.

The water mist curtain system has been studied and applied in tunnels for fire suppression and smoke control. For example, Li et al. (2013) studied the suppression effect of water mist on n-heptane pool fire in a long and narrow space with longitudinal ventilation. Sun et al., (2016) assessed the effectiveness of the water system in preventing smoke and reducing temperature through reduced-scale tunnel experiments. Bu et al. (2022) investigated the suppression performance of water mist on a train fire shielded by the carriage body by conducting fire experiments in a railway tunnel rescue station. Results showed that the direct heat loss between water mist and smoke was the main controlling mechanism.

Natural rainfall may look like the water mist curtain system, but there are big differences. First, rainfall occurs outside the tunnel and does not directly contact the fire source. Secondly, the water mist flow rate (often >6 L/(min.m^2) or 360 mm/h) is far beyond the intensity of natural rainfall between water mist and rainfall. Third, the droplet diameter of water mist is often less than 1mm (Sun et al., 2016), smaller than 0.5 - 6 mm for the diameter of raindrops (Han et al., 2021). Fourth, the water mist droplet velocity can reach 30 m/s, much faster than the raindrop terminal velocity of no more than 9

m/s (Marzuki et al., 2013). Therefore, it is important to study the impact of heavy rainfall on tunnel fire.

This study aims to assess the effect of asymmetric heavy rainfall on the smoke spread and stratification in tunnel fires through experiments in a reduced-scale tunnel model. The temperature and velocity fields of the tunnel in various fire and rainfall scenarios are quantified. Finally, the flow field inside the tunnel induced by heavy rainfall is discussed in detail to provide fire safety guidelines for real tunnels.

2. Experiment platform

2.1 Scaled tunnel model

For a buoyancy-controlled fire, the reduced-scale test based on the scaling analysis of Froude number is commonly used. Such scaled tests have also been applied to study the water mist curtain systems in tunnel fires (Yu, 2012). The scaling correlations are shown in Table 1. A reduced-scale experimental platform was built at a scale (γ) of 1:15, and its schematic diagram and the corresponding real fire scene are shown in Fig. 1. The scale of 1:15 has been used for reduced-scale tunnel fire research (Zeng et al., 2018; Han et al., 2021).

Table 1 Scaling correlations of the Froude similitude criterion

Parameters	Scaling
Length, L (m)	$L_F = \gamma L_M$
Heat release rate Q (kW)	$Q_F = \gamma^{5/2} Q_M$
Velocity V (m/s)	$V_F = \gamma^{1/2} V_M$
Energy E (KJ)	$E_F = \gamma^3 E_M$
Rainfall intensity I (mm/h)	$I_F = \gamma^{1/2} I_M$
Raindrop size d (mm)	$d_F = \gamma^{1/2} d_M$
Temperature T (K)	$T_F = T_M$

The experimental platform consisted of a scaled tunnel model and an artificial rainfall simulator. The internal dimensions of the tunnel model were 10 m in length, 0.6 m in width, and 0.4 m in height. To support the tunnel, a steel frame of 3 mm thickness was used. The bottom plate, ceiling, and back sidewall of the tunnel were built with calcium silicate boards of 20 mm thickness. The fireproof glass of 8 mm thickness was used to cover the front sidewall of the tunnel for observation and video recording. The rainfall simulator was placed outside the portal on one side of the tunnel. The effective rainfall area of 2.0 m × 2.0 m can ensure that the tunnel portal was completely enveloped by rainfall.

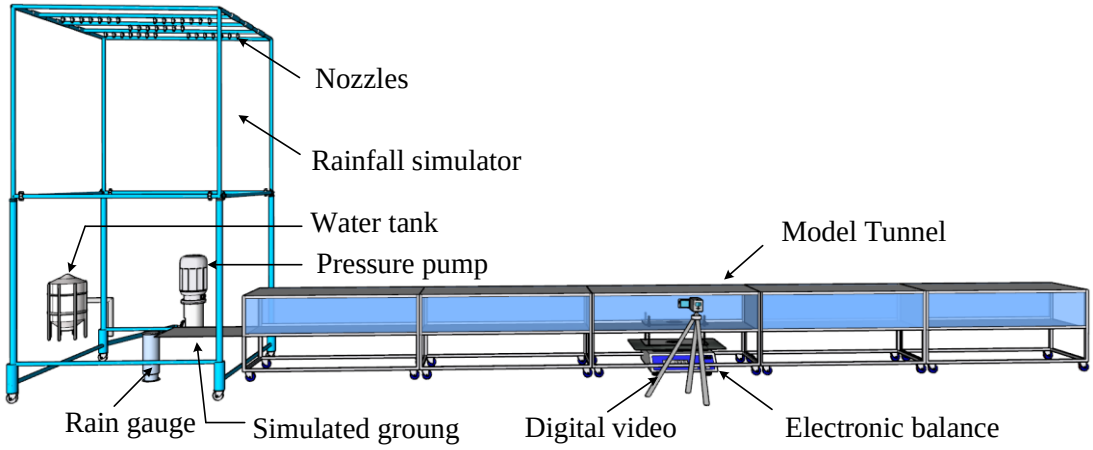

(a) Schematic of experiment platform.

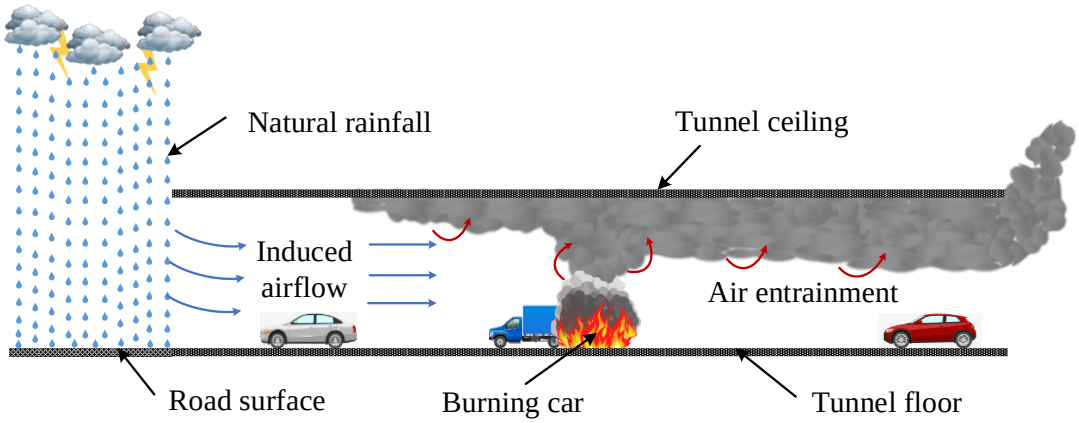

(b) The real tunnel fire scene corresponding to the test.

Fig. 1 Schematic of experiment platform and the corresponding real fire scene.

2.2 Simulated rainfall on one exit

The rainfall intensity is the key parameter to characterize rainfall. For example, there was a maximum hourly rainfall of 184.4 mm for extreme rain in Guangzhou, China, during 6-7 May 2017. The maximum hourly rainfall of 201.9 mm was recorded in Zhengzhou, China, during 17-23 July 2021. The current global record holder is 304.8 mm with 42 minutes on June 22, 1947, at Holt, Missouri, USA. Based on the Froude criterion (see Table 1), the scaled tests adopted a maximum hourly rainfall of 60 mm/h, corresponding to a rainfall intensity of 232 mm/h in nature.

The raindrop size distribution is another important characteristic of rainfall. Raindrop diameters are typically in the range of 0.5-6 mm, while exceeding 6 mm, raindrops will break into smaller ones (Han et al., 2021). Raindrop diameter generally tends to increase with increasing rainfall intensity, while its size distribution varies with climate, location, and season. In our experiments, for a given rainfall intensity, the effect of the raindrop size distribution of three median volume diameters on the smoke spread and stratification dynamics in tunnel fires was explored.

Another important parameter describing rainfall is the falling velocity. When the gravitational force of raindrops is equal to the air resistance, the terminal velocity of raindrops is reached (Serio et

al., 2019). The falling velocity varies within the range of 0.5-9 m/s (Marzuki et al., 2013). According to Covert and Jordan (2009), the design height of the water nozzle of the rainfall simulator should exceed 3 m to achieve the falling velocity and kinetic energy of real rainfall. Therefore, the nozzle height was set to 3.53 m above the simulated ground in our experiments, and the uniformity of rainfall was estimated to be greater than 88%.

The artificial rainfall simulator included nozzles, a pressure pump, a tipping bucket rain gauge, hollow pipes, a water tank, and a central controller. Thirty-five nozzles were divided into five groups and installed on the top of the bracket consisting of hollow pipes. The water pump transmits the water in the water tank to the nozzle, which distributes the water evenly to realize rainfall simulation. The real-time rainfall intensity was obtained by a tipping bucket rain gauge with an accuracy of 0.1 mm and fed back to the central controller. The central controller varied the real-time rainfall intensity to the pre-set value by adjusting the pump pressure. The real-time rainfall intensity fluctuated within 5% of the pre-set value at the stable stage. Once the rain intensity reached a stable stage, the fire inside the tunnel was ignited.

2.3 Tested tunnel fires and measurements

Hydrocarbon pool fire has been extensively employed as an experimental fire source (Yao et al., 2019). In the experiment, square pans equipped with ethanol fuel were positioned in the center of the tunnel model. Three square fuel pans with areas of 64, 100, and 144 cm^2 realized fires with heat release rates of 2.1, 4.3, and 6.7 kW without rainfall, respectively. The real size equivalents of the heat release rate were 1.8, 3.8, and 5.9 MW, respectively. In Table 2, test conditions are shown in detail. We repeated each test twice to ensure a good experimental repeatability.

The initial depths of fuel were all 8 mm, and the fuel was burnt out in the test. The mass loss history of the fuel was recorded by an electronic balance with an accuracy of 0.1g. The combustion heat of ethanol is 26.8kJ/g, and the combustion efficiency is taken as 0.994. Measured averages of the burning rate and heat release rate (HRR) of each condition are shown in Appendix A, and the equivalent HRRs in real scale is also shown. It can be found that the airflow induced by rainfall can affect the burning rate of fuel pans, which will be discussed in a separate work.

Table 2 Experimental conditions, where the steady-state fire HRR is shown.

Case No.	*Rainfall intensity* I (mm/h)	*Pool area* A (cm^2)	*Test HRR* (kW)	*Real-scale HRR* (MW)	*Mean raindrop size* d_0 (mm)
1-3	0	64, 100, 144	2.1, 4.3, 6.7	1.8, 3.8, 5.9	1.0, 1.2, 1.5
4-12	20				
13-21	30				
22-30	40				
31-39	50				
40-48	60				

Note: Test HRR shown in the table is the measured value without rainfall.

A total of 10 series thermocouple trees were symmetrically arranged along the longitudinal axis of the model tunnel on both sides of the fire source. The interval between the two thermocouple trees was arranged as 1 m, and the nearest thermocouple tree was 0.5 m away from the center of the fuel pan. In each series of thermocouple trees, 11 K-type thermocouples with a diameter of 0.1 mm were assembled. A diagram of the thermocouple arrangement is shown in Fig. 2. The ambient temperature during all tests was around 30°C.

A hand-held hot-wire anemometer (SMART SENSOR AR866A) with an accuracy of 0.01 m/s was adopted to determine the velocity of induced airflow along the model tunnel. The average velocity of the whole section is represented by the velocity of the central point of the tunnel section, and the measurement locations were selected to be 0 m, 1m, 3m, 5m, 7m, and 9m away from the tunnel portal with rainfall. A thin strip of paper was tied to the front end of the detector to determine the airflow direction. A sensor of carbon dioxide (CO_2) concentration was arranged near the no-rainfall portal, 4 m away from the center of the fuel pan and 6 cm below the tunnel ceiling.

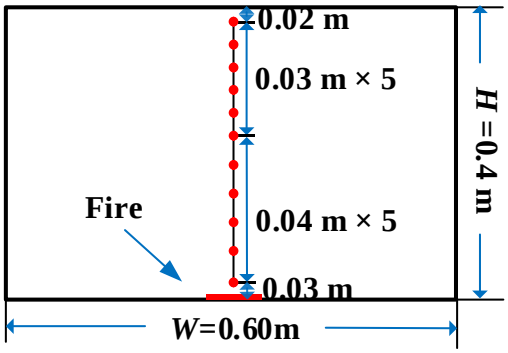

Fig. 2 Measuring point layout of thermocouple tree.

3. Results and discussion

3.1 Smoke temperature rise distribution

It is important to note that this study mainly focuses on the one-dimensional spreading stage of the smoke flow progress, that is, the temperature reaches a steady state. HRR values in the following discussion are characterized by the measured value without rainfall, and the temperature rise is discussed below rather than the temperature in order to eliminate the difference in the ambient temperature in each test. Figure 3 and Figure 4 show the mapped temperature rise distribution in the longitudinal central plane of the model tunnel under various rainfall intensities and raindrop sizes with heat release rates of 2.1 and 6.7 kW, respectively. Note that the hot fire-plume region was not captured because there was no thermocouple above the fuel pool. In the absence of rainfall (Fig. 3a and Fig. 4a), the buoyancy plume was observed vertically upward, and there was a symmetrical temperature distribution from the fire source. In addition, the high-temperature area under the tunnel ceiling is relatively large. As the rainfall intensity increases, the temperature distribution inside the tunnel

gradually becomes more asymmetrical, and the hot ceiling area becomes smaller. The phenomenon of smoke back-layering appears with increasing rainfall intensity, which seems to present an effect of wind.

Figure 5 visualizes the smoke flow regimes and the phenomenon of smoke back-layering in the tunnel by a laser sheet (taking the test of HRR=2.1 kW, d_0=1.2 mm as an example). In the absence of rainfall, the smoke stratification interface is clear and flat (Fig. 5a), while the smoke stratification interface becomes blurred and coarse under rainfall (Fig. 5b-c). With rainfall on the portal, the smoke gradually cannot escape from the tunnel portal, especially when the rainfall intensity becomes large.

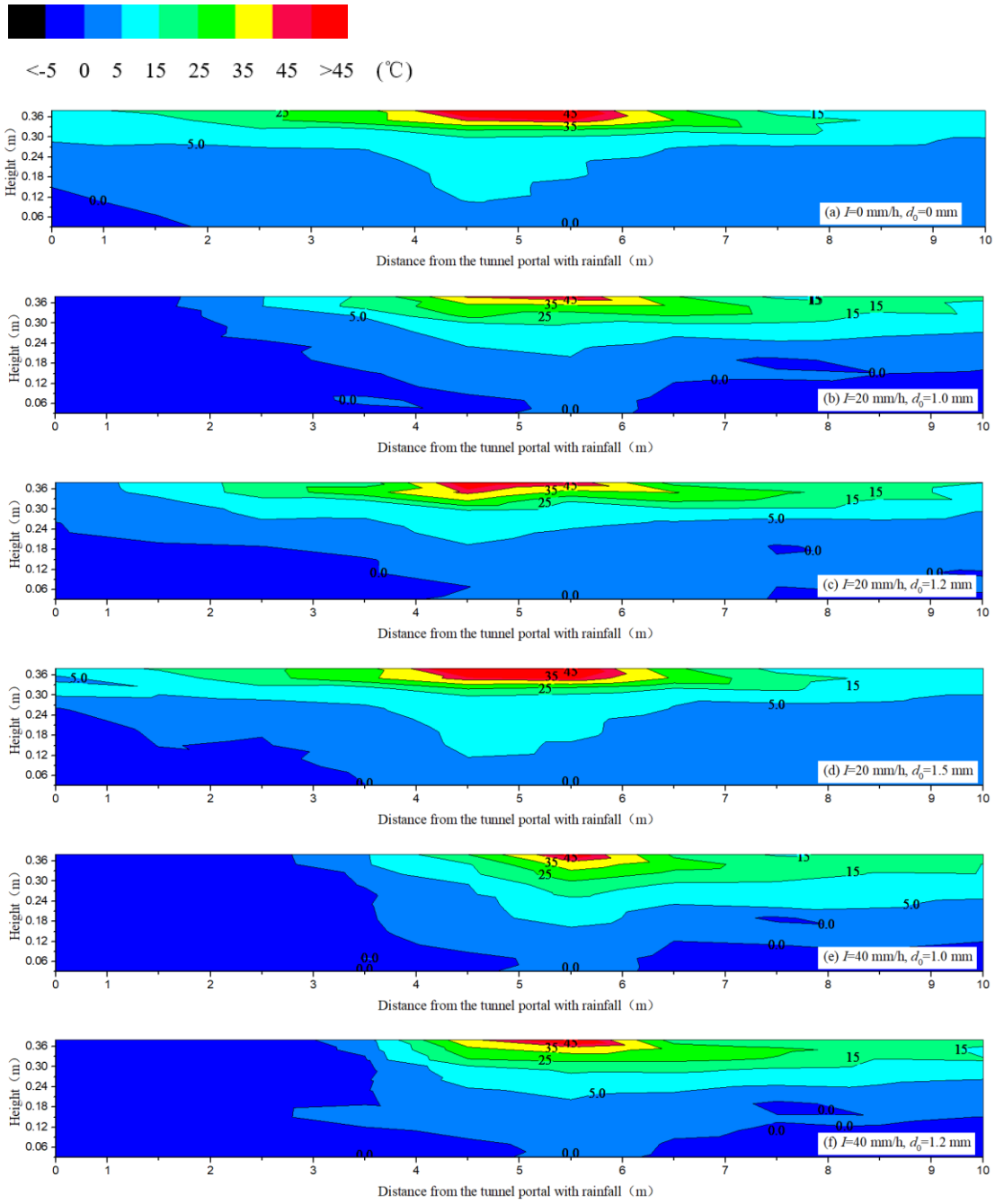

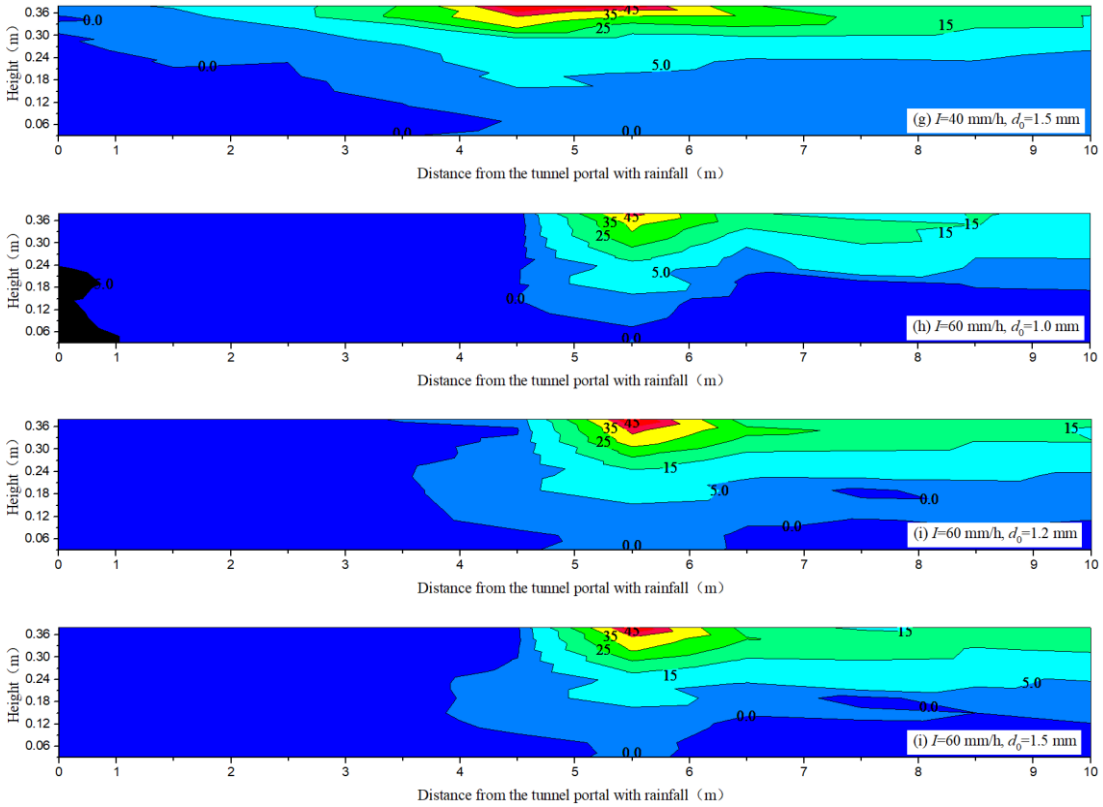

Fig. 3 Mapped temperature rise distribution in the longitudinal central plane of the model tunnel with HRR=2.1 kW.

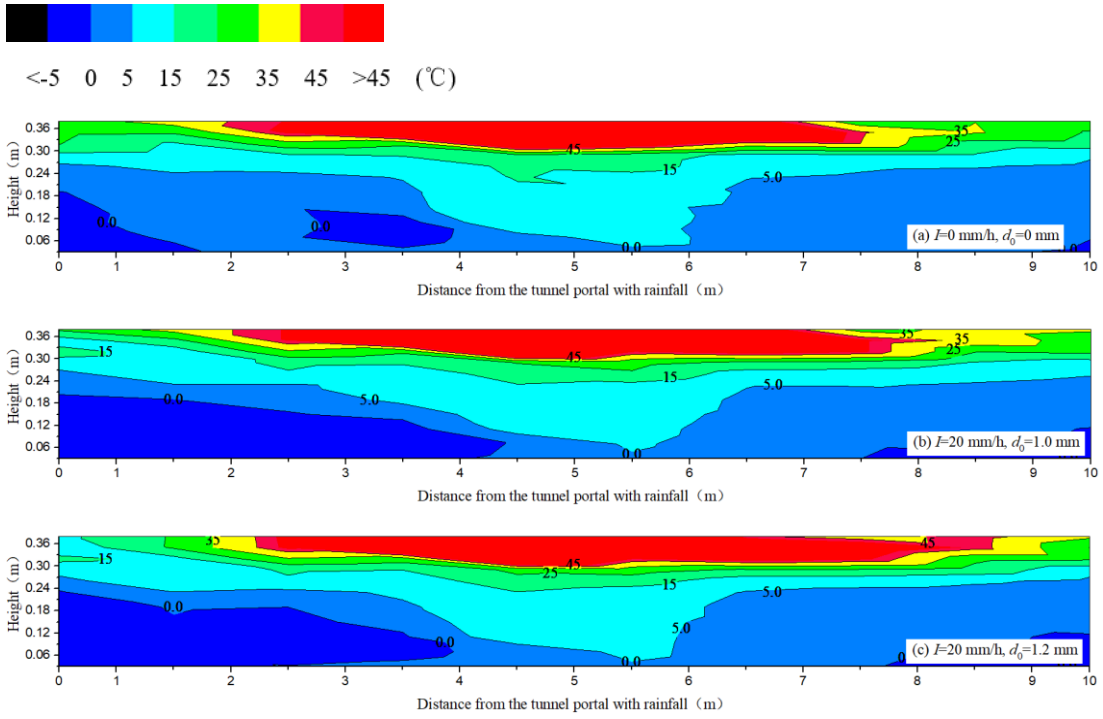

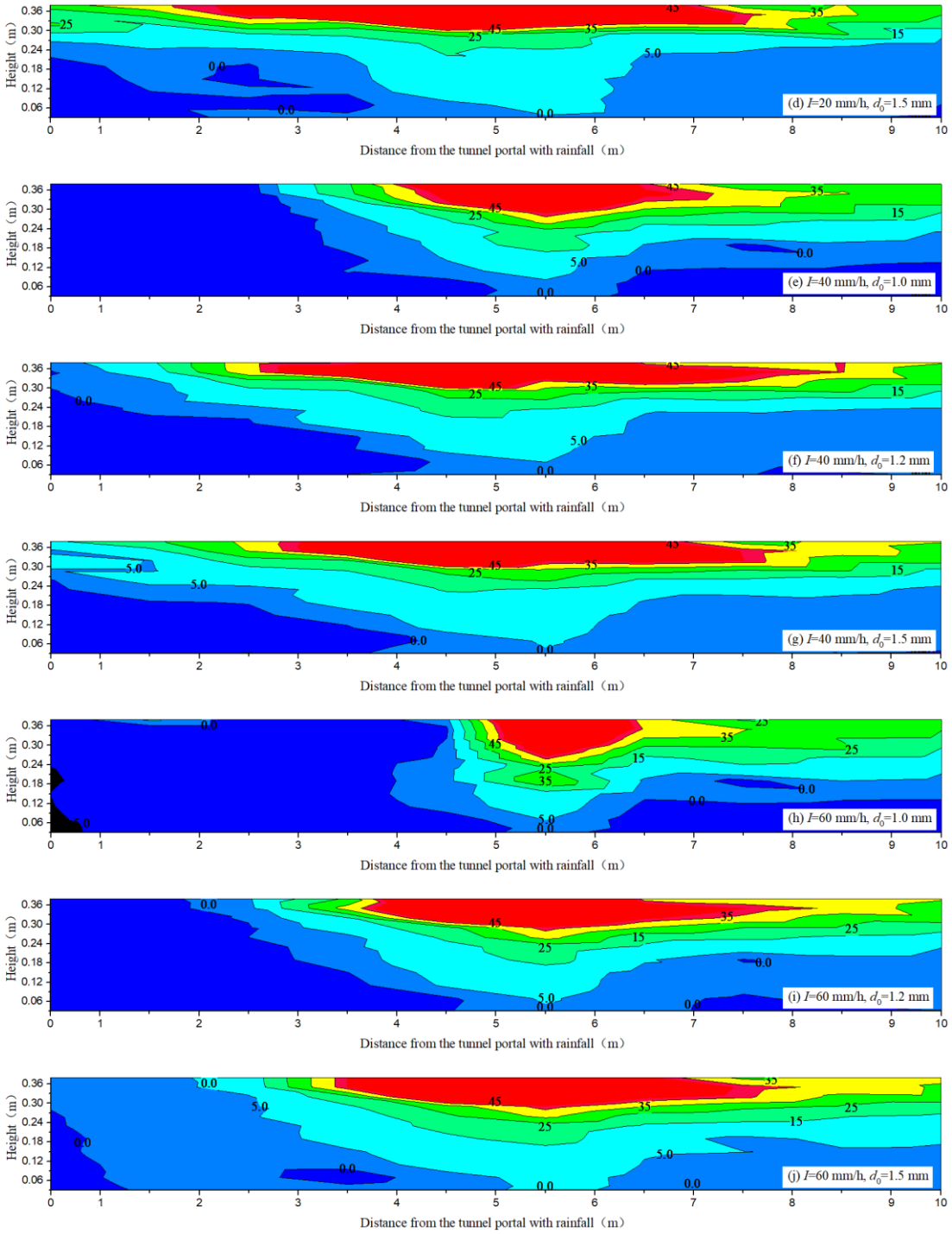

Fig. 4 Mapped temperature rise distribution in the longitudinal central plane of model tunnel with HRR=6.7 kW.

Table 3 lists the possibility of the smoke overflow through the portal with rainfall. In the absence of rainfall, the smoke can escape from both tunnel portals for all pool fires. The rainfall creates a shield to mitigate or even prevent the smoke overflow. Small raindrops can effectively reduce the chance of smoke escaping from the tunnel portal with rainfall. With increasing fire HRR, stronger rainfall intensity is required to prevent smoke from escaping from the tunnel portal with rainfall due to greater thermal buoyancy.

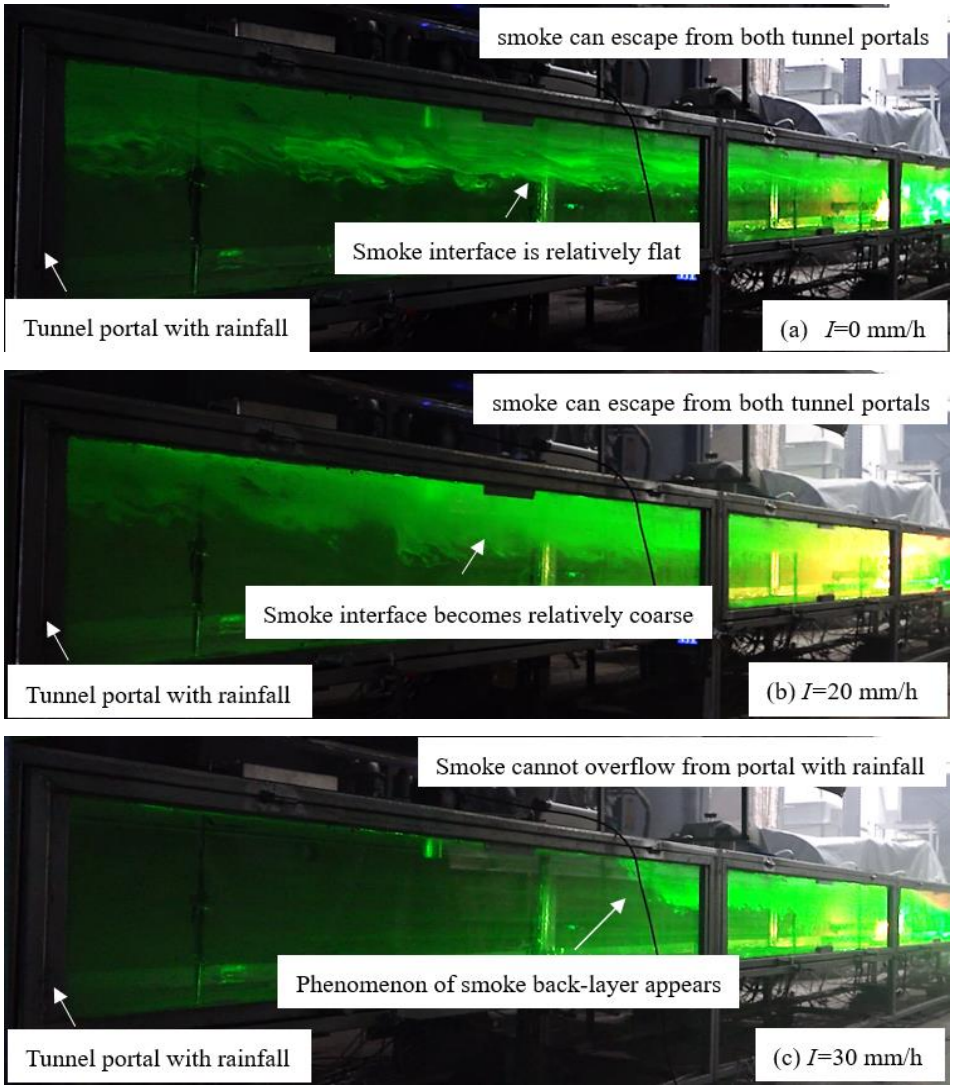

Fig. 5 Smoke flow regimes visualization.

Table 3. Possibility of smoke over-flow through the tunnel portal with rainfall.

HRR (kW)	2.1			4.3			6.7		
I (mm/h)	d_0 (mm)								
	1.0	1.2	1.5	1.0	1.2	1.5	1.0	1.2	1.5
0	Y	Y	Y	Y	Y	Y	Y	Y	Y
20	N	Y	Y	N	Y	Y	Y	Y	Y
30	N	N	Y	N	Y	Y	Y	Y	Y
40	N	N	N	N	N	Y	N	N	Y
50	N	N	N	N	N	N	N	N	Y
60	N	N	N	N	N	N	N	N	N

Figure 6 shows the longitudinal airflow in the tunnel induced by heavy rainfall on one side measured by the anemometer. The airflow inside the tunnel is induced by the following two factors. On the one hand, the longitudinal airflow is induced by the diffusion of part of the kinetic energy of raindrops hitting the ground into the tunnel. Each of these factors influences the rainfall kinetic power, including rainfall intensity, falling velocity, and raindrop size distribution. Carollo et al. (2018) found that the connection among rainfall kinetic energy (p_n), rainfall intensity (I), and median volume diameter (d_o) could be fitted by Eq. (2).

$$p_n / I = 12.53\times10^{-6}\rho\left[1-2/(1.38d_0+1)^{4.67}+1/(2.76d_0+1)^{4.67}\right] \quad (2)$$

where d_o can be used to synthesize whole information of raindrop size distribution. On the other hand, part of the air entrainment occurs after raindrops fall. These raindrops hit the ground, and then they are diffusively reflected into the tunnel, inducing longitudinal airflow. Smaller raindrop allows more air to entrain due to the larger specific surface area.

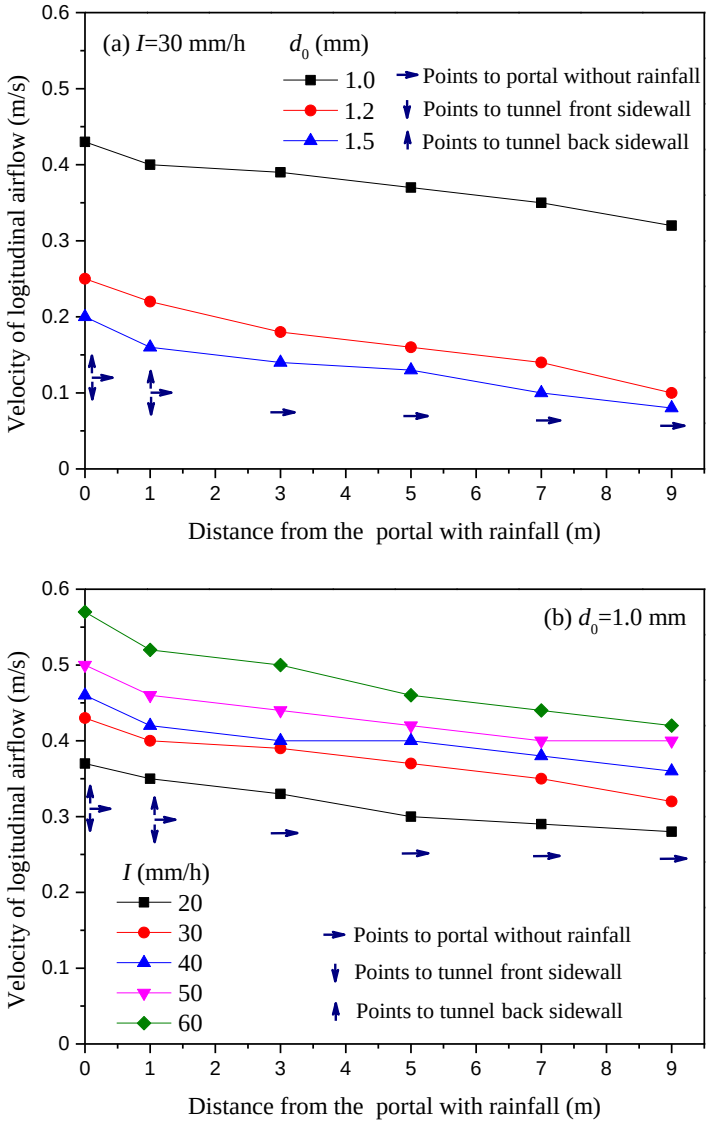

Fig. 6 Induced airflow velocity with rainfall intensity and raindrop size, where x=0 is at the portal with rainfall.

As the rainfall intensity increases, both the incident and reflected raindrop flows increase the velocity of induced airflow inside the tunnel. For a given rainfall intensity (especially smaller than 30 mm/h), the velocity of induced longitudinal airflow is larger for smaller raindrops. Further increasing the rainfall intensity above 40 mm/h (equivalent to 155 mm/h in real scale), the influence of raindrop size on induced airflow velocity becomes small. Near the rainfall portal, the paper strips swing laterally with an angle of less than 10°. By moving away from the rainfall portal, strips tilt steadily towards the other portal, which means stable longitudinal airflow is induced. In addition to the longitudinal airflow induced by rainfall on one portal, Figures 3-6 also show that smoke spread and stratification are very sensitive to the induced airflow.

3.2 Vertical temperature rise profile

Taking the tests of HRR=2.1 kW as instances, Figure 7 shows the dimensionless vertical temperature rise profiles at 0.5 m and 4.5 m away from the fire source towards the no-rainfall portal under various rainfall intensities and raindrop sizes. The curve presents two different gradients, representing the temperature decay of the smoke layer and the air layer, respectively. A greater gradient difference indicates more obvious smoke stratification. The demarcation point of temperature decay gradients was defined by the boundary between the decay of the smoke layer and the air layer.

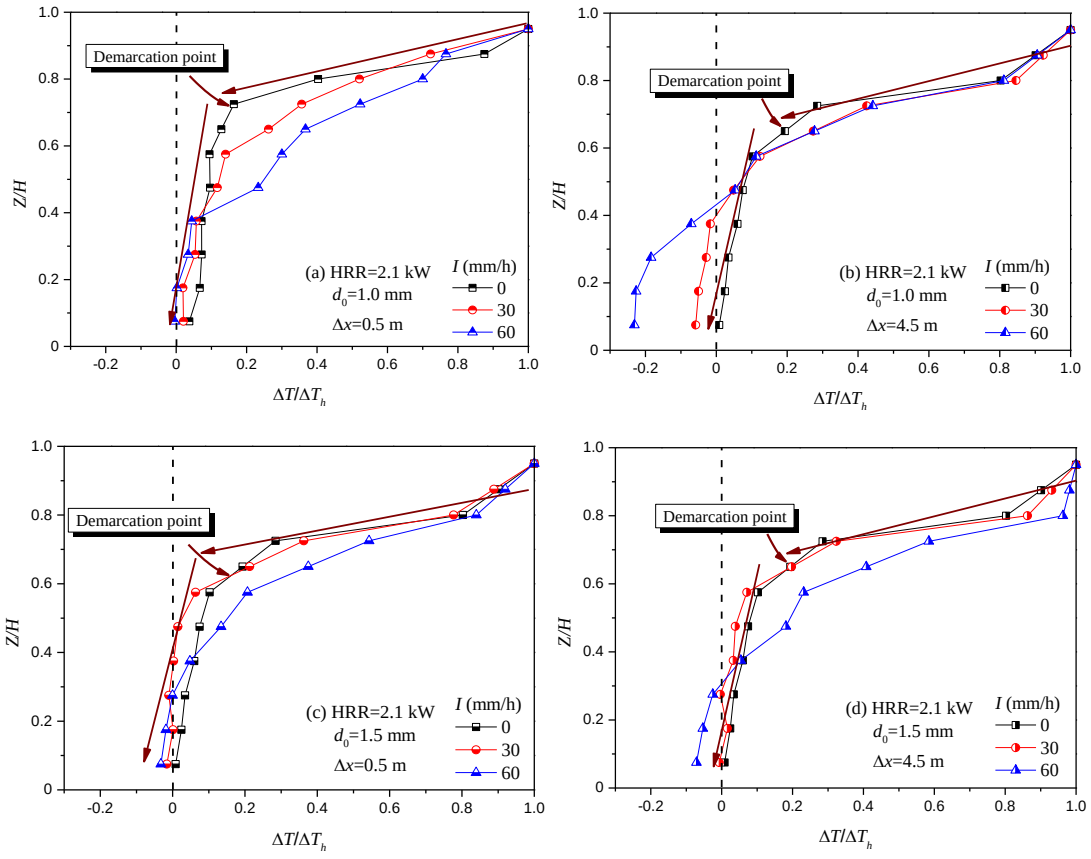

Fig. 7. Vertical temperature rise profiles with rainfall intensity and raindrop size.

In the absence of rainfall, the hot smoke region is thin, and the temperature gradient shows a sharp change, which implies the clear smoke stratification in the tunnel. With increasing rainfall intensity, the thickness of the hot smoke layer generally increases. Moreover, the temperature change is more smooth, and the boundary between the upper hot smoke layer and lower cold air layer becomes unclear or blurred because the mixing of smoke and air is more intense. There are two mechanisms. Firstly, the rainfall-induced airflow enhances the convective heat transfer between hot and cold layers, so the vertical temperature distribution becomes uniform. Such a convective mixing increases with the rainfall intensity. Secondly, smaller raindrops are easier to evaporate, which can further enhance the heat and mass transfer between hot smoke and cold fresh air.

3.3 Smoke layer height

According to statistics, 85% of fire victims died of smoke inhalation. Fire safety researchers have been keen to determine the smoke layer height (Oka et al., 2016; Xu et al., 2019b). To determine the smoke layer heights, N-percentage, buoyancy frequency, and integral methods are all commonly used.

Cooper et al. (1982) developed the N-percentage method and prescribed the smoke layer height as the location where the excess temperature reached N% of the maximum excess temperature. The selection of N values is subjective, and 10, 20, and 30 are the most commonly used. When the temperature decay gradient is relatively small, the selection of N values has a large effect on the determination of the interface height. The interface height can be determined by Eq. (3):

$$T_i - T_0 = (T_{\max} - T_0) \times N/100 \tag{3}$$

The buoyancy frequency method assumes that the fluid has a strong density gradient, so it is not suitable to be used in the case of poor stratification. The integral ratio method presented by He et al. (1998) is an objective method that reflects the optimal location of stratification between the hot airflow and the cold airflow. For the integral ratio method, calculating the interface height can be done by Eqs. (4) and (5).

$$r = r_u + r_l = 1/(H - H_i)^2 \int_{H_i}^{H} T(z)dy \int_{H_i}^{H} [1/T(z)]dy + 1/H_i^2 \int_{0}^{H_i} T(z)dy \int_{0}^{H_i} [1/T(z)]dy \tag{4}$$

$$r(H_i) = \min(r_t) \tag{5}$$

Comparing to the above methods, the integral ratio method was found to be the best approach for quantifying the smoke layer height. The smoke layer interface of a typical test is determined by the integral ratio, as shown in Fig. 8. Figure 9 shows the smoke layer height at positions of 0.5 m and 4.5 m away from the fire source towards the no-rainfall portal under various rainfall intensities and raindrop sizes. Due to the increasing amount of air entrained by the smoke, the smoke layer height constantly decrease as the rainfall intensity increases.

Raindrop size has a stronger impact on smoke layer heights due to the less stable smoke layer where relatively close to the fire source, and a smaller raindrop size means a lower smoke layer height. As the distance from from the fire source increases, the smoke layer tends to stabilize, and the influence of the raindrop size on the smoke layer height decreases. Especially, for the relatively small pools (HRR=2.1 kW and 4.3 kW), the height of the smoke layer increases when the rainfall intensity increases from 50 mm/h to 60 mm/h with Δx = 4.5 m and d_0= 1.0 mm. The reason may be that the hot smoke is accelerated by the induced airflow with an increased velocity, which promotes smoke to discharge from the no-rainfall portal.

Figure 10 shows the data from the CO_2 concentration monitoring device under different rainfall intensities and raindrop sizes. It can be found that under rainfall conditions, the concentration of CO_2 at the monitoring position decreases because the smoke layer is diluted by the entrained air, which also means that the smoke fills the space in the lower part of the tunnel. As the rainfall intensity increases, the CO_2 concentration at the monitoring position continues to decrease, and the smoke filling becomes more obvious, which endangers the fire evacuation. For the same rainfall intensity, a smaller raindrop size means more intense air entrainment and more serious smoke filling.

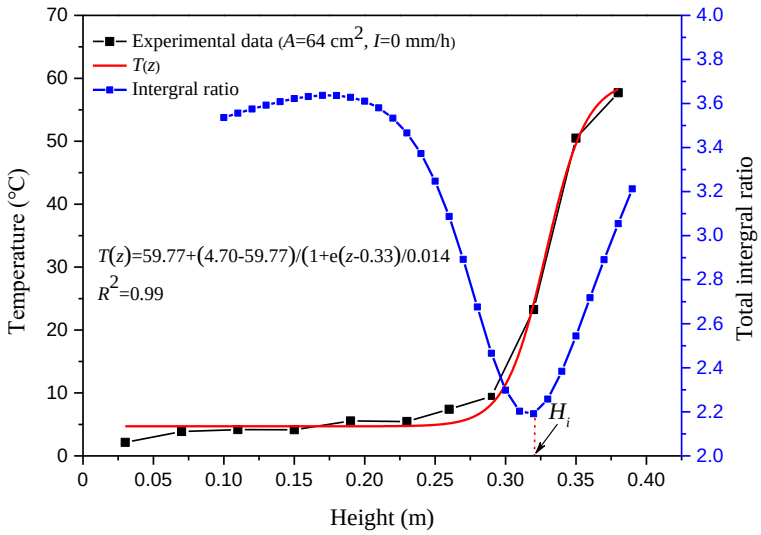

Fig. 8 Smoke layer interface of a typical test determined by the integral ratio.

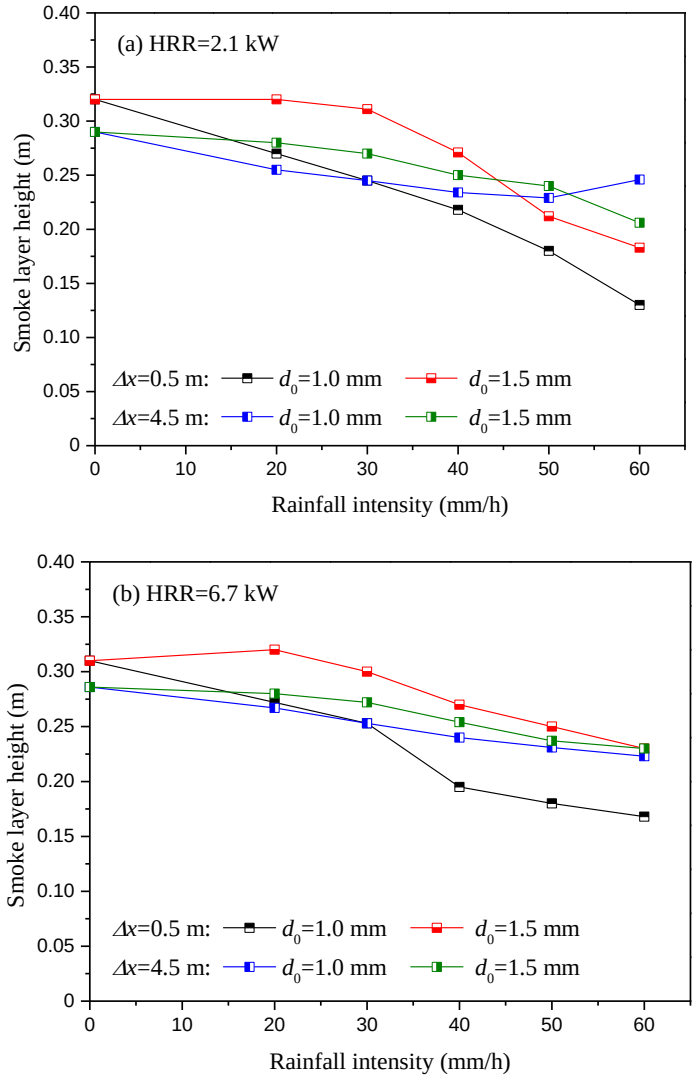

Fig. 9 Smoke layer height with rainfall intensity and raindrop size.

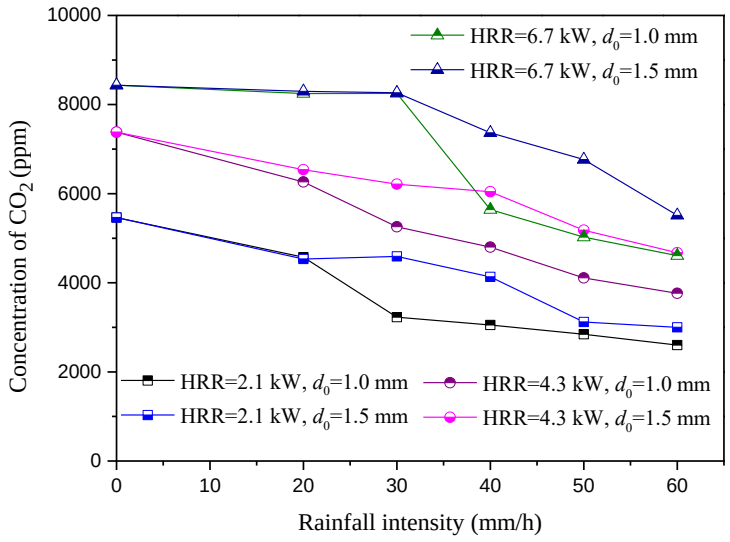

Fig. 10 Data of CO_2 concentration with rainfall intensity and raindrop size.

4. Conclusions

Multiple model tests were performed to assess the smoke spread and stratification characteristics during tunnel fires under the impact of asymmetric heavy rainfall. The following are the main conclusions:

(1) Asymmetric heavy rainfall will induce longitudinal airflow inside the tunnel due to the diffusion of the rainfall kinetic energy and air entrained by raindrops. The induced airflow velocity increases with increasing rainfall intensity, and smaller raindrops mean larger induced airflow velocity for given rainfall intensity. When rainfall intensity reaches 40 mm/h (equivalent to 155 mm/h in nature), the influence of raindrop size on induced longitudinal airflow velocity decreases.

(2) Under rainfall conditions, the longitudinal temperature distribution inside the tunnel gradually is no longer symmetrical, and the smoke layer interface becomes coarser. With increasing rainfall intensity, the phenomenon of smoke back-layering gradually appears. Under the impact of the induced airflow, the gradient difference in vertical temperature decay between the smoke layer and the air layer decreased, indicating that the mixing of smoke and air is more intensive.

(3) With the rainfall intensity increasing, the smoke layer height constantly decreases due to the increasing amount of entrained air, and the smoke fills the space in the lower part of the tunnel. Under a low rainfall intensity and a close distance from the fire source, raindrop size has a strong influence on smoke layer heights.

Acknowledgments

This work was supported by the National Natural Science Foundation of China (Grant No. 52278545), and Central South University Research Programme of Advanced Interdisciplinary Studies (Grant No. 2023QYJC024).

References

Bu, R.W., Fan, C.G., Guo, Z.W., Zhou, Y., 2022. Energy distribution analysis on suppressing a shielded fire with water mist in a tunnel rescue station. Process Saf. Environ. Prot. 158, 409-417.

Carollo, F.G., Ferro, V., Serio, M.A., 2018. Predicting rainfall erosivity by momentum and kinetic energy in mediterranean environment. J. Hydrol. 560, 173-183.

Cooper, L.Y., Harkleroad, M., Quintiere, J., 1982. An experimental study of upper hot layer stratification in fullScale multiroom fire scenarios. Int. J. Heat Mass Transf. 104, 741-749.

Covert, A., Jordan, P., 2009. A portable rainfall simulator techniques for understanding the effects of rainfall on soil erodibility. Streamline Watershed Managment Bulletin, 13, 5-9.

C. Fan, D. Luan, R. Bu, Z. Sheng, F. Wang, X. Huang (2023) Can heavy rainfall affect the burning and smoke spreading characteristics of fire in tunnels? International Journal of Heat and Mass Transfer (under review).

Gao, Z.H., Li, L.J., Sun, C.P., Zhong, W., Yan, C.B., 2022. Effect of longitudinal slope on the smoke propagation and ceiling temperature characterization in sloping tunnel fires under natural ventilation. Tunn. Undergr. Space Technol. 123, 104396.

Guo, Y.H., Yuan, Z.Y., Yuan, Y.P., Gao, X.L., Zhao, P., 2021. Numerical simulation of smoke stratification in tunnel fires under longitudinal velocities. Undergr. Space 6, 163-172.

Han, J.Q., Wang, F., Wang, Z.H., Geng, P.Q., Liu, F., Weng, M.C., 2021. Experimental investigation on the fire and thermal smoke spread in tunnels: Effects of fire elevation. Tunn. Undergr. Space Technol. 118, 104192.

Han, Y., Guo, J.P., Yun, Y.X., Li, J., Guo, X.R., Lv, Y.M., Wang, D., Li, L., Zhang, Y., 2021. Regional variability of summertime raindrop size distribution from a network of disdrometers in Beijing. Atmos. Res. 257, 105591.

He, Y.P., Fernando, A., Luo, M.C., 1998. Determination of interface height from measured parameter profile in enclosure fire experiment. Fire Saf. J. 31, 19-38.

Hu, L. H., Peng, W., Huo, R., 2008. Critical wind velocity for arresting upwind gas and smoke dispersion induced by near-wall fire in a road tunnel. J. Hazard. Mater. 150, 68-75.

IPCC, 2022. Impacts of 1.5ºC Global Warming on Natural and Human Systems. PP. 175-312.

Ji, J., Guo, F.Y., Gao, Z.H., Zhu, J.P., 2018. Effects of ambient pressure on transport characteristics of thermal-driven smoke flow in a tunnel. Int. J. Therm. Sci. 125, 210-217.

Ji, J., Guo, F.Y., Gao, Z.H., Zhu, J.P., Sun, J.H., 2017. Numerical investigation on the effect of ambient pressure on smoke movement and temperature distribution in tunnel fires. Appl. Therm. Eng. 118, 663-669.

Kunsch, J. P., 1999. Critical velocity and range of a fire-gas plume in a ventilated tunnel. Atmospheric Environ. 33, 13-24.

Lemaire, T., Kenyon, Y., 2006. Large Scale Fire Tests in the Second Benelux Tunnel. Fire Technol.42, 329-350.

Li, Q.W., Zhang, P., Guo, S., Pan, R.M., Qin, J., Liao, G.X., 2013. Experimental study on suppression of n-heptane pool fire with water mist under longitudinal ventilation in long and narrow spaces. Procedia Eng. 62, 946- 953.

Luan, D., Yi, L., Yang, L.L., Chen, T., Tao, H.W., Xu Z.S., Fan, C.G., 2021. Experimental investigation of smoke temperature and movement characteristics in tunnel fires with canyon cross wind. J.

Wind Eng. Ind. Aerod. 210, 104531.

Marzuki, Randeu, W.L., Kozu, T., Shimomai, T., Hashiguchi, H., Schönhuber, M., 2013. Raindrop axis ratios, fall velocities and size distribution over Sumatra from 2D-Video Disdrometer measurement. Atmos. Res. 119, 23-37.

Ministry of Transport of the People's Republic of China, 2022. Specifications for Design of Highway Underwater Tunnel. PP. 104-108.

Motevalli, V., Marks, C., 1991. Characterizing the unconfined ceiling jet under steady-state conditions: A Reassessment. Fire Saf. Sci. 3, 301-312.

Newman, J.S., 1984. Experimental evaluation of fire-induced stratification. Combust. Flame 57, 33-39.

Oka, Y., Oka, H., Imazeki, O., 2016. Ceiling-jet thickness and vertical distribution along flat-ceilinged horizontal tunnel with natural ventilation. Tunn. Undergr. Space Technol. 53, 68-77.

Serio, M.A., Carollo F.G., Ferro, V., 2019. Raindrop size distribution and terminal velocity for rainfall erosivity studies. A review. J. Hydrol. 576, 210-228.

Sun, J.Y., Fang, Z., Tang, Z., Beji, T., Merci, B., 2016. Experimental study of the effectiveness of a water system in blocking fire-induced smoke and heat in reduced-scale tunnel tests. Tunn. Undergr. Space Technol. 56, 34-44.

Tabari, H., 2020. Climate change impact on flood and extreme precipitation increases with water availability. Sci. Rep. 10, 13768.

Weng, M.C., Lu, X.L., Liu, F., Shi, X.P., Yu, L.X., 2015. Prediction of backlayering length and critical velocity in metro tunnel fires. Tunn. Undergr. Space Technol. 47, 64-72.

Wu, F., Zhou, R., Shen, G.S., Jiang, J.C., Li, K.Y., 2018. Effects of ambient pressure on smoke back-layering in subway tunnel fires. Tunn. Undergr. Space Technol. 79, 134-142.

Xu, Z.S., Liu, Q.L., He, L., Tao, H.W., Zhao, J.M., Chen, H.G., Li, L.J., Fan, C.G., 2019a. Study on the heat exhaust coefficient and smoke flow characteristics under lateral smoke exhaust in tunnel fires. Fire Mater. 43, 857-867.

Xu, Z.S., Zhao, J.M., Liu, Q.L., Chen, H.G., Liu, Y.H., Geng, Z.Y., He, L., 2019b. Experimental investigation on smoke spread characteristics and smoke layer height in tunnels. Fire Mater. 43, 303-309.

Yan, Z.G., Guo, Q.H., Zhu, H.H., 2017. Full-scale experiments on fire characteristics of road tunnel at high altitude. Tunn. Undergr. Space Technol. 66, 134-146.

Yang, D., Li, P., Duan, H., Yang, C., Du, T., Zhang, Z.J., 2019. Multiple patterns of heat and mass flow induced by the competition of forced longitudinal ventilation and stack effect in sloping tunnels. Int. J. Therm. Sci. 138, 35-46.

Yao, Y.Z., Li, Y.Z., Ingason, H., Cheng, X.D., 2019. The characteristics of under-ventilated pool fires in both model and medium-scale tunnels. Tunn. Undergr. Space Technol. 87, 27-40.

Yu, H.Z., 2012. Froude-modeling-based general scaling relationships for fire suppression by water sprays. Fire Saf. J. 47, 1-7.

Zeng, Z., Xiong, K., Lu, X.L., Weng, M.C., Liu, F., 2018. Study on the smoke stratification length under longitudinal ventilation in tunnel fires. Int. J. Therm. Sci. 132, 285-295.

Zhang, X.N., Wu, X.Q., Park, Y., Zhang, T.H., Huang, X.Y., 2021. Perspectives of big experimental database and artificial intelligence in tunnel fire research. Tunn. Undergr. Space Technol. Trenchless Technol. 108, 103691.

Appendix A

Case No.	Pool area A (cm^2)	Mean raindrop size d_0 (mm)	Rainfall intensity I (mm/h)	Burning Rate (g/s)	Test HRR (kW)	Real-scale HRR(MW)
1	64	-	-	0.0782	2.0821	1.8144
2	100	-	-	0.1619	4.3116	3.7572
3	144	-	-	0.2530	6.7408	5.8741
4	64	1.0	20	0.0878	2.3506	2.0382
5	64	1.2	20	0.0882	2.0635	1.7982
6	64	1.5	20	0.0828	2.2052	1.9217
7	100	1.0	20	0.1581	4.2109	3.6694
8	100	1.2	20	0.1738	4.6291	4.0339
9	100	1.5	20	0.1519	4.0462	3.5260
10	144	1.0	20	0.2609	6.9496	6.0561
11	144	1.2	20	0.2752	7.3300	6.3878
12	144	1.5	20	0.2445	6.5125	5.6751
13	64	1.0	30	0.0831	2.2132	1.9287
14	64	1.2	30	0.0972	2.5891	2.2561
15	64	1.5	30	0.0878	2.3395	2.0387
16	100	1.0	30	0.1545	4.1155	3.5863
17	100	1.2	30	0.1801	4.7967	4.1799
18	100	1.5	30	0.1656	4.4107	3.8435
19	144	1.0	30	0.2559	6.8180	5.9414
20	144	1.2	30	0.2677	7.1302	6.2134
21	144	1.5	30	0.2567	6.8393	5.9600
22	64	1.0	40	0.0834	2.2209	1.9353
23	64	1.2	40	0.0941	2.5070	2.1845
24	64	1.5	40	0.0863	2.2990	2.0034
25	100	1.0	40	0.1398	3.7250	3.2460
26	100	1.2	40	0.1754	4.6725	4.0712
27	100	1.5	40	0.1614	4.3004	3.7474
28	144	1.0	40	0.1897	5.0535	4.4037
29	144	1.2	40	0.2516	6.7024	5.8041
30	144	1.5	40	0.2135	5.6875	4.9562
31	64	1.0	50	0.0876	2.3328	2.0328
32	64	1.2	50	0.0854	2.2758	1.9832
33	64	1.5	50	0.0805	2.1442	1.8685
34	100	1.0	50	0.1384	3.6866	3.2126
35	100	1.2	50	0.1614	4.2985	3.7459
36	100	1.5	50	0.1357	3.6032	3.1400
37	144	1.0	50	0.1920	5.1147	4.4571
38	144	1.2	50	0.2067	6.5714	5.7264
39	144	1.5	50	0.2048	5.4544	4.7531
40	64	1.0	60	0.0963	2.5659	2.2360
41	64	1.2	60	0.0913	2.4324	2.11978
42	64	1.5	60	0.0984	2.6200	2.2831
43	100	1.0	60	0.1569	4.1805	3.6430
44	100	1.2	60	0.1486	3.9591	3.4501
45	100	1.5	60	0.1353	3.6046	3.1411
46	144	1.0	60	0.1847	4.9211	4.2883
47	144	1.2	60	0.2261	6.0234	5.2490
48	144	1.5	60	0.1795	4.7825	4.1676